Distinct and dynamic distributions of multiple elements and their species in the rice rhizosphere

YUAN, ZF, GUSTAVE, W, ATA-UL-KARIM, ST, BRIDGE, Jonathan <http://orcid.org/0000-0003-3717-519X>, SEKAR, R, LIU, F and CHEN, Z <http://orcid.org/0000-0002-1184-3682>

Title: Distinct and dynamic distributions of multiple elements and their species in the rice rhizosphere

Names of authors:

Zhao-Feng Yuan [1,2,3], Williamson Gustave [1,2,4], Syed Tahir Ata-Ul-Karim [5], Jonathan Bridge [6], Raju Sekar [7], Fuyuan Liu [8] and Zheng Chen [1 *]

[1] Department of Health and Environmental Sciences, Xi'an Jiaotong-Liverpool University, 111 Ren'ai Road, Suzhou, Jiangsu 215123, China.

[2] Department of Environmental Science, University of Liverpool, Brownlow Hill, Liverpool L69 7ZX, UK.

[3] MOE Key Lab of Environmental Remediation and Ecosystem Health, College of Environmental and Resource Sciences, Zhejiang University, Hangzhou 310058, China.

[4] Chemistry, Environmental & Life Sciences, University of The Bahamas, New Providence, Nassau, The Bahamas.

[5] Department of Global Agricultural Studies, Graduate School of Agricultural and Life Sciences, The University of Tokyo, Tokyo 113-8654, Japan.

[6] Department of Natural and Built Environment, Sheffield Hallam University, Howard St, Sheffield S1 1WB, UK.

[7] Department of Biological Sciences, Xi'an Jiaotong-Liverpool University, 111 Ren'ai Road, Suzhou, Jiangsu 215123, China.

[8] Department of Electric and Electronic, School of Advanced Technology, Xi'an Jiaotong-Liverpool University, 111 Ren'ai Road, Suzhou, Jiangsu 215123, China.

[*] **Corresponding author**: Zheng Chen (E-mail: ebiogeochem@outlook.com or Zheng.Chen@xjtlu.edu.cn; Tel: +86-512-81880471; fax: +86-512-88161899).

Abstract

Aims The biogeochemical cycles of elements from soils to plants are mainly governed by their rhizosphere processes. Understanding these processes is challenging and remains largely unresolved due to the complex interrelationships among different elements and due to a lack of appropriate techniques for simultaneous spatiotemporal monitoring.

Methods This study employed an updated *In-situ* Porewater Iterative (IPI) sampler to collect porewater across the rice rhizosphere at a spatial resolution of 1.7 mm and a time interval of 3-10 days. An IPI sampler array (0-22 mm measurement distance every 1.7 mm) was adopted to capture the *in situ* spatiotemporal dynamics of ten elements (Fe, Mn, As, P, S, Cr, Co, Zn, Sb and Cd) in the paddy rhizosphere to examine their covarying changes in time and space dimensions, with an emphasis on As and Cd.

Results The findings revealed that the solute-phase concentration of most elements, other than Sb and Cd, increased to a peak after 30 days of paddy soil flooding and then decreased. Additionally, Sb and Cd continuously decreased during flooding. Fe (-52%), Mn (-17%), P (-43%), Co (-11%), and As species (-74%) were substantially immobilized within a 10 mm zone around the roots, while Zn (28%) and Cd (41%) increased. Almost all arsenite-oxidizing genes were significantly promoted in the rhizosphere.

Conclusions Our study showed most sampled elements covaried with Fe both in time and space in the rhizosphere, but the elements are temporally and spatially determined by multiple biogeochemical processes in soils as well as exudates from plant roots.

Keywords: rice rhizosphere, spatiotemporal, multiple elements, arsenic, cadmium

TOC art

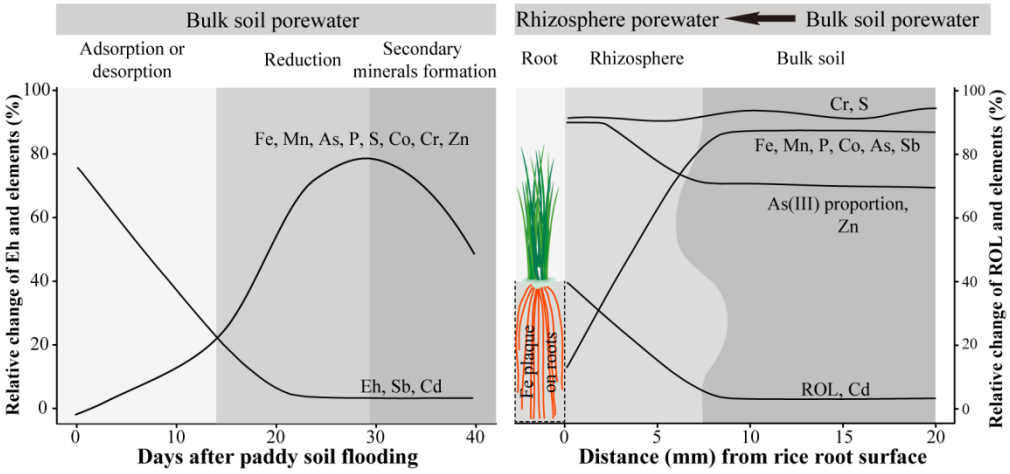

Introduction

The ability of rice to adapt in order to grow under diverse conditions (aerobic and anaerobic) gives it a unique status among crops. This diversity results in differences in biogeochemical reactions that alter the interactions between soil chemistry and rice roots (Kuzyakov and Razavi 2019). Oxygen (O_2) in paddy soils under flooded conditions is rapidly consumed by microbes during the rice growth period, and the passive transportation of atmospheric O_2 through aerenchymatous tissues enables rice to withstand hypoxic conditions (Revsbech et al. 1999). O_2, other than that respired by rice roots, is released by roots as radial oxygen loss (ROL), which results in significant deposition of iron (Fe) in the rhizosphere after reacting with the abundant ferrous Fe ions (Fe^{2+}) in soil porewater (Chen et al. 2005). The microbial community, nutrient availability, pollutant mobility, and greenhouse gas emissions in paddy soils are greatly influenced by alterations in rhizosphere characteristics as a consequence of ROL-induced oxidizing areas (Kuzyakov and Razavi 2019), which may extend approximately 10-25 mm from the root surface (Maisch et al. 2019). The elucidation of all indigenous processes occurring in the rice rhizosphere is imperative for improving soil and rice quality. However, a thorough description of these processes remains largely unresolved.

Rhizospheric processes are strongly influenced by the formation of Fe oxides around rice roots (i.e., Fe plaque) in paddy soils, owing to the diversified role of Fe plaque as a barrier (Chen et al. 2005; Martin et al. 2019) and/or facilitator (Richardson et al. 2009; Yin et al. 2020) of mineral uptake. The barrier effect is mainly due to the high affinity of Fe oxides, which have a high surface area and rich functional groups capable of binding with anions and cations (Hansel et al. 2001; Suda and Makino 2016). Many studies have reported that Fe plaques inhibit arsenic (As) (Chen et al.

2005), phosphorus (P) (Zhang et al. 1999), lead (Ma et al. 2012), copper (Ye et al. 2001), nickel (Ni) (Xu et al. 2015), and cadmium (Cd) (Liu et al. 2007) uptake by plants. However, the function of the Fe plaques may be reversed when other processes are involved. The coupling of Fe^{2+} oxidization with proton release leads to acidification of the rhizosphere (Kuzyakov and Razavi 2019; Maisch et al. 2019), which in turn enhances metal ion bioavailability through their desorption from solid minerals (Wang et al. 2019). Furthermore, in reducing paddy soils, sulfides (S(-II)) are produced by sulfate (S(VI))-reducing bacteria and form metal/metalloid S(-II) (Arsic et al. 2018; Borch et al. 2010; Pester et al. 2012). The S(-II) of metals/metalloids (e.g., copper, Cd, mercury, antimony (Sb) and As) are not readily available for plant uptake owing to their extremely low solubility. Sulfur (S)-oxidizing bacteria exposed to the ROL-inducing oxic rhizosphere use rich electron acceptors (Martin et al. 2019; Thomas et al. 2014), including O_2, nitrate and Fe oxides, to oxidize reducing S and remobilize the metals/metalloids. The rhizosphere acidification and release of root exudates tend to enhance metal/metalloid remobilization in the rhizosphere (Kuzyakov and Razavi 2019). Assessing element behaviours in the paddy rhizosphere is difficult due to complex interactions among elements that are dependent on the chemical nature, root functions, rhizosphere, and microbial activity of the elements. Consequently, it is plausible to speculate that different elements have different spatial distributions in the paddy rhizosphere, and a detailed examination of their distribution in the rhizosphere is required for an in-depth understanding of the processes occurring in the rice root-soil system.

The chemical gradients in the paddy rhizosphere swiftly change in time and space. The distribution of oxidized areas along the entire active roots has been evaluated by using electrochemical probes and planar optodes, but the highest O_2

concentrations were observed in the 2-4 mm region around the tips of young roots (Williams et al. 2014; Yin et al. 2020). In contrast, solute-phase Fe^{2+} exhibits an opposite trend to O_2, namely, Fe^{2+} is low on the root surface (Maisch et al. 2019). Fine mapping of trace elements in the paddy rhizosphere has rarely been investigated. A new hotspot of greatly enhanced fluxes of As, Pb and Fe(II) adjacent to rice root tips (within a few mm) using diffusive gradients in thin films (DGT) has been documented (Williams et al. 2014). However, the root tips have a weak impact on cobalt (Co), manganese (Mn), zinc (Zn), and Ni (Yin et al. 2020). DGT, despite being a very powerful tool for generating 2D spatial maps of elements, can only take a snapshot at a certain time interval. Conversely, other soil solution samplers, such as microsuction cups, can be used for repeated measurements but cannot be used to map the chemical gradient (Brackin et al. 2017; Seeberg‐Elverfeldt et al. 2005). To date, the measurements cannot probe the dynamics of the rhizosphere at a sufficient resolution; they are fixed (or limited) either in time or in space. Consequently, a detailed understanding of the spatiotemporal changes in elements in the paddy rhizosphere remains dubious due to the lack of appropriate techniques for mapping the dynamic distribution of elements in the paddy rhizosphere.

This study aimed to reveal the complex processes of soluble elements in the paddy rhizosphere by applying a tool called Rhizon profiler. The profiler was based on the In-*situ* Porewater Iterative (IPI) sampler developed by our group (Yuan et al. 2019), which can repeatedly collect porewater with ultralow disturbance of the soil matrix. Being coupled with ICP-MS or IC-ICP-MS (Yuan et al. 2020; Yuan et al. 2019), this sampler can provide a two-dimensional (space and time) map of elements and/or their species in porewater across the paddy rhizosphere. The two dimensions of the Rhizon profilers are a spatial dimension (0-22 mm distance from the root bag

surface) with a resolution of 1.7 mm and a time dimension with a resolution of 24 hours. This updated sampler can act as a powerful tool to identify hotspots and hot moments in the rhizosphere. This study focused on As and Cd due to their higher accumulation in rice grains and the health risk associated with their dietary intake. However, due to the presence of P, S, Zn, Fe, Mn, Cr, Co, and Sb in paddy soils (Eberle et al. 2020; Shaheen et al. 2014; Wan et al. 2019; Wang et al. 2019; Zhang et al. 1999), their potential association with As and Cd behaviors in flooded soils was also investigated in this study.

We hypothesized that (1) most elements in the paddy rhizosphere covary with Fe in time and space owing to the high adsorption capacity of Fe oxides and (2) the ROL-induced zone hosts distinct species distributions mediated by microbes. Four As species (arsenite (As(III)), arsenate (As(V)), monomethylarsonic acid (MMA), and dimethylarsinic acid (DMA)) are common in paddy soils (Guo et al. 2020; Kumarathilaka et al. 2018; Muehe et al. 2019). As(V) is reduced to As(III) when soils become reducing and is further methylated to DMA when anaerobic microorganisms possessing the capacity for As methylation thrive. The demethylation process driven by methanogens dominates under continuously decreasing Eh (Chen et al. 2019a). The transformation of As species may actively occur in the paddy rhizosphere (Afroz et al. 2019). The availability of electron acceptors and donors makes the paddy rhizosphere a potential hotspot for the transformation of elemental species; however, sampling along the redox gradient in the rhizosphere has been a major challenge. This study endeavored to test these hypotheses with real contaminated paddy soils by profiling the elements at different distances from roots.

Materials and methods

Experimental preparation

As-contaminated paddy soil was collected from Shaoguan (25°6'N, 113°38'E), China. The topsoil layer (0-20 cm) was sampled followed by wet sieving to remove stones and plant debris through a 1.0 mm diameter sieve. The selected soil properties are depicted in Table S1. The rice hybrid Yliangyou-1, with a medium level of ROL (according to the Fe plaque formation, 56.8 g Fe kg^{-1}) (Chen et al. 2019b), was sterilized and germinated following the method described in a previous report (Chen et al. 2012). The seedlings were grown in a Hoagland culture in a glass greenhouse from 30 March 2019 to 1 May 2019 (three-leaf stage) before being transplanted into the soils. The plants were grown in a glass greenhouse under natural light, and the temperature was set and controlled at 25/20 °C days/night controlled by an air conditioner.

Porewater sampling by Rhizon profilers

The IPI sampler used in this study shares the same design as in a recent report by our group (Yuan et al. 2021). The structure of an IPI sampler is shown in Fig. 1A. The IPI sampler includes three components: (1) the hollow fiber membrane tube (modified polyethersulfone, 20 nm pore size, inner × outer diameter × length = 1.0 mm × 1.7 mm × 35 mm, 27.5 μL, Motimo Membrane Technology Co., Ltd., Tianjin, China); (2) two pipes (PTFE, inner × outer diameter × length = 0.5 mm × 1.0 mm × 180 mm, 35 μL); and (3) two silicon caps (inner × outer diameter × depth × length = 1.0 mm × 2.0 mm × 10 mm × 20 mm). When the IPI sampler is deployed into solution or saturated soils, solutes around the hollow fiber membrane tube can diffuse through the membrane (Fig. 1A). The solution inside the tube is pumped out and collected when the diffusion reaches equilibrium (24 hours) (Yuan et al. 2019; Yuan et al. 2021). During deployment, silicon caps are applied to seal the IPI sampler to avoid potential

185 contamination (e.g., gasoline fumes) from the atmosphere. During each sampling
186 event, a 27.5 μL liquid sample in the sampling tube was mixed with 70 μL ultrapure
187 water in the pipes when they were pumped out from the sampler. This indicates that
188 an approximately 100 μL porewater sample can be collected each time by the IPI
189 sampler, with a dilution factor of 3.5.

190 One big advantage of the IPI sampler is its disturbance to the porewater is very
191 small. Firstly, porewater sampling by IPI samplers is non-destructive. Secondly, IPI
192 samplers do not induce porewater flow in soils. Thirdly, the disturbance of IPI
193 samplers to the porewater can be further reduced by decreasing the sampling
194 frequency. In addition, to accurately take the porewater samples, three counter
195 measures were undertaken in this study: i) IPI samplers are horizontally assembled,
196 which can avoid the influence of vertically elemental diffusion along the soil profile;
197 ii) the sampling equilibrium can be quickly completed in the sampler (3-24 hours),
198 during which changes of elements outside the sampler would be very small; iii) IPI
199 samplers do not remove porewater from the soil, thus elemental migration driven by
200 water flow is eliminated. Therefore, IPI samplers could serve as a powerful tool to
201 study elemental changes at the micro-interface.

202 Horizontally assembled IPI samplers were designed to measure a sampling zone
203 across the rhizosphere at a sufficient resolution (mm level) (Fig. 1B). To achieve this,
204 thirteen IPI samplers were horizontally assembled in a 3D printed holder (Fig. 1C).
205 The IPI sampler array, i.e., the Rhizon profiler, after being combined with a nylon
206 mesh bag (nominal pore size = 37 μm, height × width = 10 mm × 8 cm), is able to
207 collect porewater *in situ* at a 0-22 mm distance from the root bag surface every 1.7
208 mm, and the rhizosphere soils can be destructively collected from a soil slot adjacent
209 to the porewater samplers (Fig. 1C). When deploying the Rhizon profiler and root bag

into the soils incubated in the pot in this study, well-mixed wet soils (3000 g; 100% moisture) were added into a black plastic bucket (inner diameter × height = 15-18 cm × 21 cm) with a soil depth of approximately 15 cm, and 600 g of the total 3000 g was enclosed in the root bag. The Rhizon profiler along with the root bag was buried at approximately 8 cm depth below the soil-water interface followed by the addition of ultrapure water to maintain a 3-5 cm overlying water depth during the experiment.

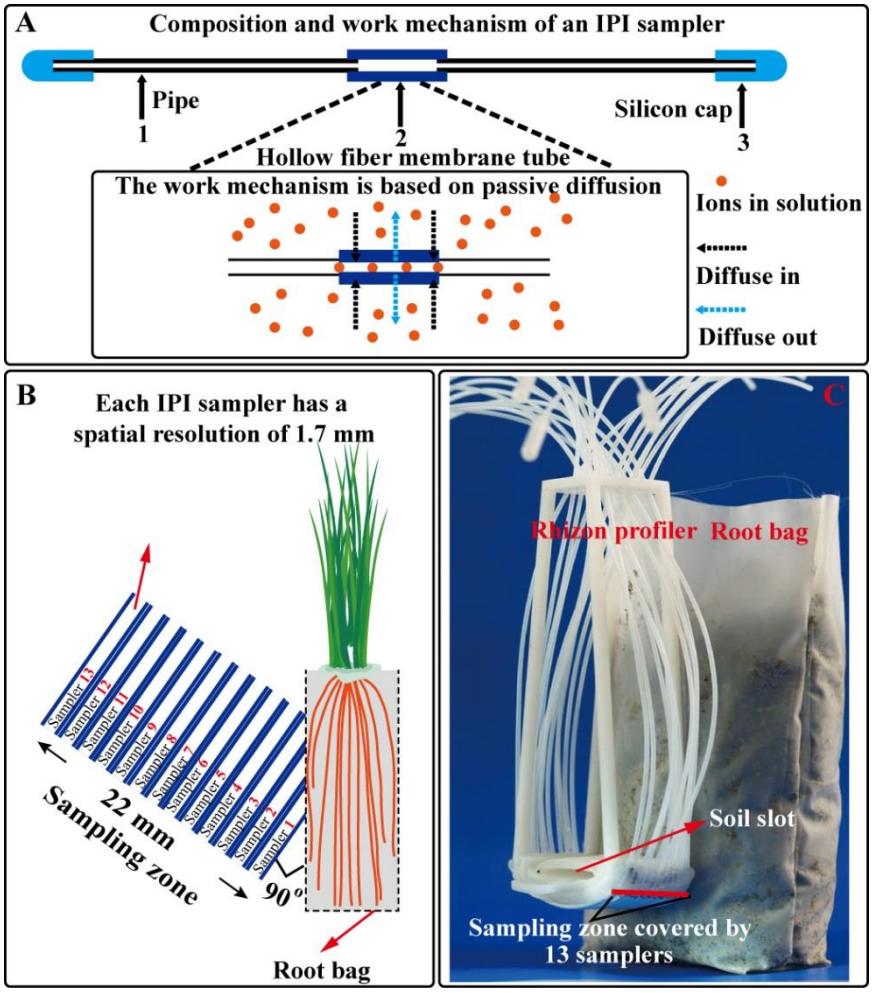

Figure 1 Porewater across the rice rhizosphere sampled by 13 *In-situ* Porewater Iterative (IPI) samplers assembled in each Rhizon profiler. A) a typical IPI sampler; B) conceptual diagram of using an IPI sampler array to sample porewaters across the rice rhizosphere; C) real photo of the IPI array, i.e., Rhizon profiler combined with a root bag.

In situ multielement measurement across the rhizosphere

A pot experiment with three replicates was conducted with (treatment)/without (control) rice growing into the root bag (Fig. S1). Two seedlings were transplanted into each root bag of the treatment group upon the soil flooding. The pots were placed in a glass greenhouse at randomly selected locations. The positions of the pots were switched every other day during the experiment to minimize the potential influence of the external environment. Porewater was sampled *in situ* across 0-22 mm from the root bag by Rhizon profilers at days after paddy soil flooding (DAF) 0, 3, 8, 15, 24, 30 and 40 with or without rice growing in root bags. Multielement information in each 100 μL porewater sample was determined by the high-throughput analytical method developed by our group (Yuan et al. 2021). Total solute-phase Fe, Mn P, S, As, Cd, Sb, Cr, Co and Zn preserved with HCl were measured by inductively coupled plasma-mass spectrometry (ICP-MS, NexION 350X, PerkinElmer, Inc., Shelton, CT USA) with data only analysis. The $^{57}Fe^{+}$, $^{55}Mn^{+}$, $^{47}PO^{+}$, $^{48}SO^{+}$, $^{91}AsO^{+}$, $^{111}Cd^{+}$, $^{121}Sb^{+}$, $^{52}Cr^{+}$, $^{59}Co^{+}$ and $^{66}Zn^{+}$ counts were recorded in a dynamic reaction cell (DRC, O_2 as the reaction gas) or extended dynamic range (EDR) mode simultaneously. The limits of detection (LOD) for Fe, Mn, P, S, As, Cd, Sb, Cr, Co and Zn were 210, 1.56, 7.76, 60.2, 0.490, 0.127, 0.129, 0.535, 0.124, 1.77 μg L^{-1}, respectively. The sample taken at DAF 40, preserved with EDTA, was used to measure As [As(III), As(V), MMA, DMA] and S [S(VI), S(-II)] species by coupling ion chromatography (IC, Dionex ICS-1100, Thermo Scientific, USA) with ICP-MS using the NH_4HCO_3 mobile phase (20 mM, pH = 10) (Suzuki et al. 2009; Yuan et al. 2021). A spiked standard was tested after every 30 samples to assure data quality.

Plant and microbial analysis

247 Multiple elements in plant tissues and the microbial community in the
248 rhizosphere were investigated at the jointing stage (DAF 40). The Rhizon profilers
249 and root bags were retrieved from the soils after porewater sampling at DAF 40. The
250 rice plants were removed from the root bags, and their roots were gently cleaned with
251 ultrapure water. The Fe plaque was not separated from rice roots, thus elements in Fe
252 plaque and roots were pooled as the elemental concentration in roots in this study.
253 The fresh plants were separated into roots, stems and leaves, followed by oven-drying
254 (60 °C) (Zhang et al. 1999) and freeze-drying (-85 °C) (Hansel et al. 2001) of
255 subsamples for the subsequent determination of total elements and As species,
256 respectively. Plant samples after oven-drying were weighed to measure the plant dry
257 matter, followed by grinding and sieving through a 1.0 mm sieve for chemical
258 analysis. A sample of 0.5 g was digested using a 1:1 mixture of concentrated HNO_3
259 and H_2O_2 (Gustave et al. 2019). The digested samples were filtered through a 0.45 μm
260 cellulose filter and diluted with ultrapure water. The total Fe, Mn, P, S, As, Cd, Sb,
261 Cr, Co and Zn were measured by ICP-MS. Freeze-dried ground samples (0.2 g) were
262 extracted with a modified protein extraction solution (Quaghebeur et al. 2003). The
263 extracted samples were filtered through a 0.45 μm pore size filter and measured by
264 IC-ICP-MS. Spiked standards were tested to assure data quality.
265 Soils at 0-2 mm from the root bags (the soils were deposited within a slot on a
266 Rhizon profiler, Fig. 1C) were instantly sampled at the time of retrieving the root bag
267 from the soils to assess the effects of the rhizosphere on the microbial community.
268 The soil genomic DNA extraction and next-generation DNA sequencing are detailed
269 in the supplementary information. The 16S rRNA gene sequence data were deployed
270 in NCBI GenBank (SUB8907191). The alpha and beta diversity analyses were
271 performed in QIIME 1.8.0. Indices of Chao 1, Shannon, Simpson, and Good's

coverage were selected for the alpha diversity analysis. The beta diversity index and principal coordinates analysis (PCoA) were applied to calculate the differences between samples. The changes in the microbial community were further evaluated using linear discriminant analysis (LDA) effect size (LEfSe) (Gustave et al. 2019; Segata et al. 2011). In addition, high-throughput qPCR reactions were performed to identify As metabolic genes using Wafergen SmartChip Real-time reactions (Chen et al. 2016). Soil DNA was analyzed by high-throughput qPCR AsChip as reported by Zhao et al. (2019). Nineteen As genes, including As(III) oxidation (*aoxA*/*B*/*C*/*D*/*R*/*S*/*H*, and *arxA*), As(V) reduction (*arrA*/*B*, and *arsC*/*R*), As methylation and demethylation (*arsM* and *arsI*), and As transport (*arsA*/*B*/*D*/*P*, and *acr3*), were quantified.

Statistical analysis

The element information was extracted from the raw data files acquired by ICP-MS analysis using R software (version 3.5.0) (Yuan et al. 2019). In addition, R software was also used to plot the graphs. Data from different treatments were subjected to one-way analysis of variance (ANOVA) to determine statistical significance ($p < 0.05$) using SPSS 22 software (IBM SPSS, Armonk, NY, USA). For multielement comparisons and to indicate their differences in the root bag surroundings and in the bulk soils, their concentrations in 0-1.7, 1.7-3.4, 3.4-5.1, 5.1-6.8, 6.8-8.5, 8.5-10 mm and 10-22 mm distances were selected. Microbial variation in the 0-2 mm distance from the root bag between the treatment and control was compared to show the shift of the microbial community in the rhizosphere. The potential bias of the element supply from porewater [soluble elements in bulk soil ($Element_{10\text{-}22\ mm}$) *vs.* in the narrow zone around roots ($Element_{0\text{-}1.7\ mm}$)] to roots was calculated with ($Element_{10\text{-}22\ mm}$ - $Element_{0\text{-}1.7\ mm}$)/$Element_{0\text{-}1.7\ mm}$*100. Translocation

coefficients of the element from the bulk soil to rhizosphere (T_{bs-r}) [$Element_{10-22\ mm}$ *vs.* $Element_{0-1.7\ mm}$], rhizosphere to root (T_{r-r}) [$Element_{0-1.7\ mm}$ *vs.* the element concentration in root ($Element_{root}$)], root to stem (T_{r-s}) [$Element_{root}$ *vs.* the element concentration in stem ($Element_{stem}$)], stem to leaf (T_{s-l}) [$Element_{stem}$ *vs.* the element concentration in leaf ($Element_{leaf}$)], and bulk soil to leaf ($T_{overall}$) ($Element_{10-22\ mm}$ *vs.* $Element_{leaf}$) were calculated with $Element_{0-1.7\ mm}/Element_{10-22\ mm}$, $Element_{root}/Element_{0-1.7\ mm}$, $(Element_{stem} + Element_{leaf})/(Element_{root} + Element_{stem} + Element_{leaf})$, $Element_{leaf}/(Element_{stem} + Element_{leaf})$, and $Element_{leaf}/Element_{10-22\ mm}$, respectively. Elemental concentrations in porewater and plant tissues were presented in μg/mg L^{-1} and mg/g kg^{-1}, respectively.

Results

Spatiotemporal changes of multiple solute elements across the rhizosphere

In this study, the temporal-spatial variation in solute-phase elements across the rice rhizosphere was mapped at DAF 0, 3, 8, 15, 24, 30 and 40 with or without growing rice in the root bags. We monitored Fe, Mn, P, As, S, Cd, Sb, Cr, Co and Zn *in situ* across 0-22 mm from the root surface with a spatial resolution of 1.7 mm. Considerable temporal-spatial variation in the elements was observed across the rhizosphere (Fig. 2).

The solute-phase concentrations of the elements in bulk soil porewater varied with the flooding period and could be clustered into 3 groups, as shown in the control without growing rice in the root bags (Fig. S2). Group 1 includes Fe, Mn, P, As, S, and Co. In group 1, solute-phase Fe increased from 2.59 mg·L^{-1} at DAF 0 to a peak of 42.3 mg·L^{-1} at DAF 30 and then decreased to 15.9 mg·L^{-1} at DAF 40 (Fig. S2A). All the elements in group 1 shared a similar temporal pattern with Fe. Group 2 includes 2

322 elements (Cr and Zn), which also increased initially and dropped like group 1, but an
323 increase of solute-phase Cr and Zn quickly started from DAF 3, and the high values
324 were maintained for approximately one month before declining. Cd and Sb are the
325 group 3. The elements in group 3 decreased rapidly after flooding (Fig. S2G&F).
326 Solute-phase Sb decreased dramatically from 74.6 $\mu g \cdot L^{-1}$ at DAF 0 to an average of
327 30.4 $\mu g \cdot L^{-1}$ after DAF 3 (Fig. S2G). More significantly, solute-phase Cd decreased
328 approximately 10-fold after DAF 3 (1.45 $\mu g \cdot L^{-1}$) compared to that in DAF 0 (10.4
329 $\mu g \cdot L^{-1}$, Fig. S2G). The correlation analysis vividly demonstrates the covarying
330 changes of the elements. Fig. 1K&S2K illustrate that the changes in Fe, Mn, P, As, S,
331 Cr, Co and Zn were not covaried with Cd and Sb, especially for Cd (r = -0.42),
332 showing that the behaviors of the elements in group 3 were distinct from those in
333 groups 1 and 2 (Fig. S2).

334 Rice roots have strong effects on the spatiotemporal changes in elements in the
335 rhizosphere (Fig. 2). In the absence of rice roots, there was no apparent spatial pattern
336 of those elements (Fig. S2). Solute-phase Fe, Mn, P, As, Co and Sb were immobilized
337 in the presence of rice roots beginning at DAF 15 (Fig. 2A-D&I). During root
338 development, the immobilization zone extended from 0-2 to 0-10 mm from the root
339 bag surface, except for Sb. The immobilization of Sb only occurred <2 mm from the
340 root bag surface. In contrast, solute-phase Cd and Zn were substantially promoted in
341 the rhizosphere from DAF 8 (Fig. 2F&J). Additionally, the mobilization zone of Zn
342 was much larger than that of Cd. The high Zn zone extended to 10 mm from the root
343 bag surface, and the mobilization zone of Cd was restricted to <2 mm. The roots had
344 weak and insignificant effects on S and Cr (Fig. 2E&H).

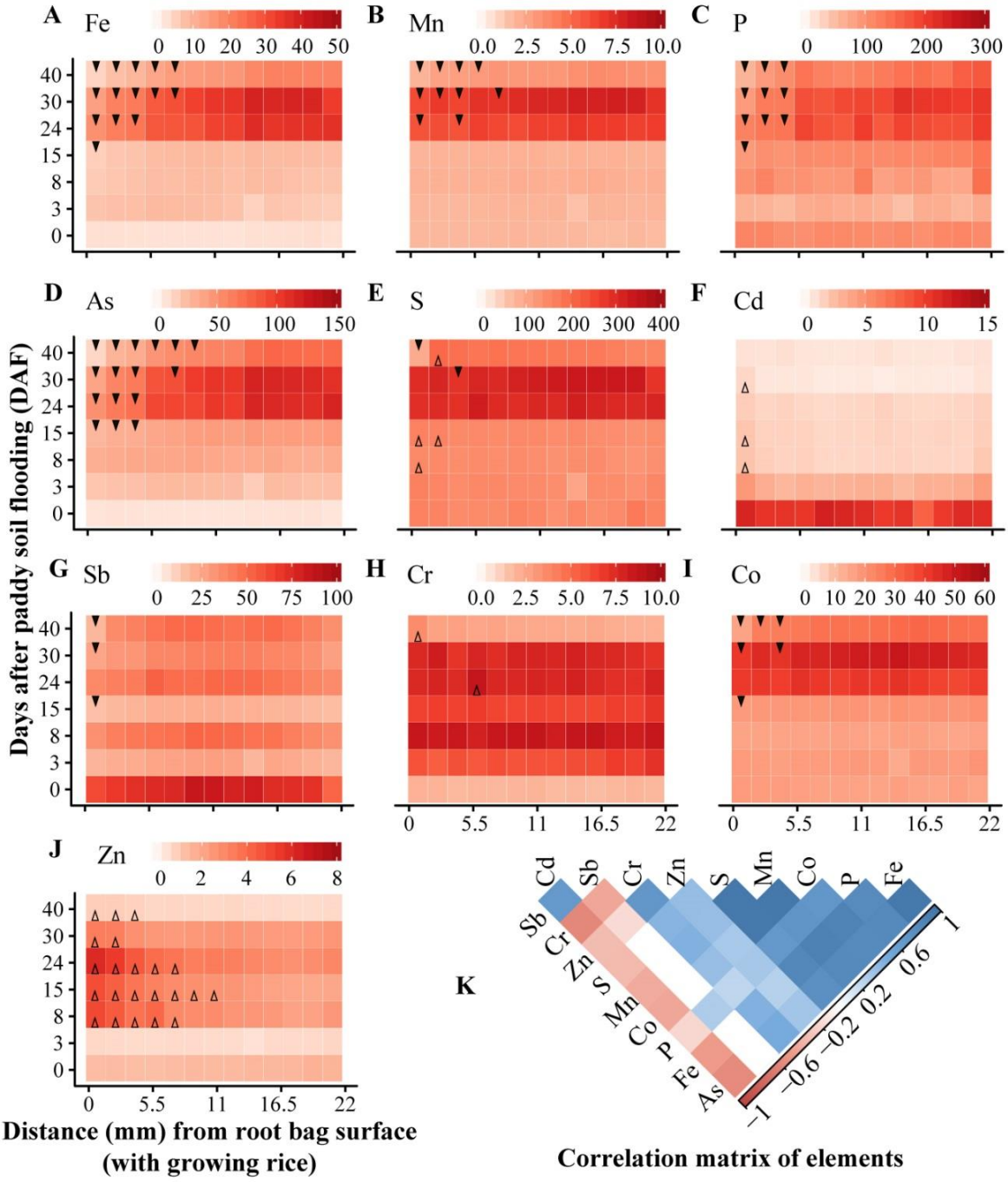

345

346 **Figure 2** Profiles of multiple elements across the rhizosphere at days after paddy soil
347 flooding (DAF) 0-40 with rice growing in root bags. A-J: Heatmaps of Fe (mg·L^{-1},
348 A), Mn (mg·L^{-1}, B), P (μg·L^{-1}, C), As (μg·L^{-1}, D), S (mg·L^{-1}, E), Cd (μg·L^{-1}, F), Sb
349 (μg·L^{-1}, G), Cr (μg·L^{-1}, H), Co (μg·L^{-1}, I), Zn (μg·L^{-1}, J), with the down-direction
350 solid triangle and up-direction hollow triangle indicating significantly lower or higher,
351 respectively, compared to that of the control group ($p < 0.05$, $n = 3$). K: Correlation
352 matrix of elements in the rhizosphere (0-10 mm, $n = 147$).

Speciation of As and S across the rhizosphere and the driving factors

To interpret the potential biogeochemical mechanisms involved in regulating As and S redox in the rice rhizosphere, their speciation across the rhizosphere and associated driving factors were investigated. Among the common As and S species, only 2 As (As(V) and As(III)) and one S species (S(VI)) were detected in the soil porewater, while methyl As and S(-II) were not detected.

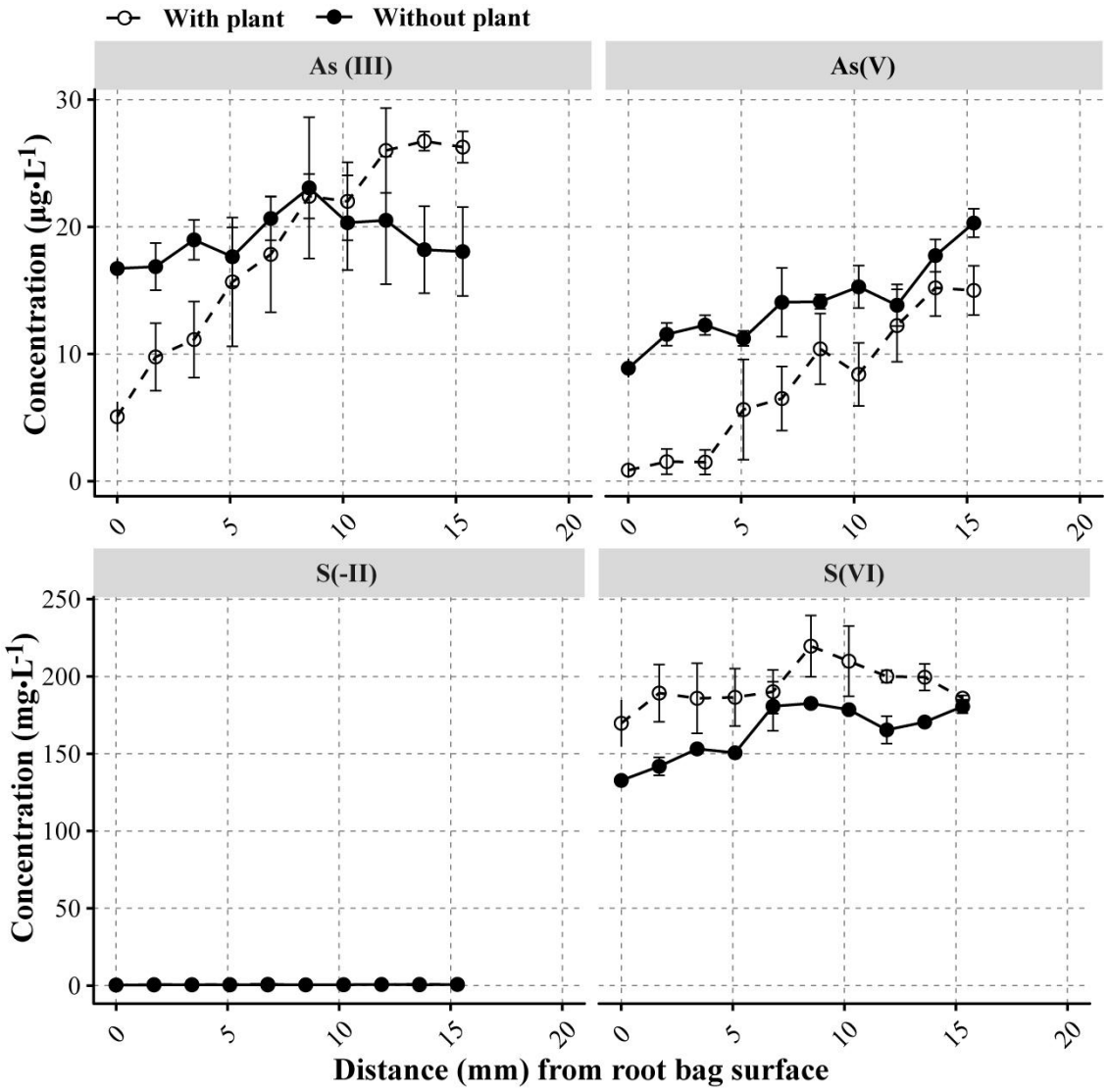

Figure 3 Spatial changes in As and S species across the rhizosphere (0-15 mm) at DAF 40. Arsenic and S species include arsenite [As(III)] and arsenate [As(V)] and sulfide [S(-II)] and sulfate [S(VI)], respectively. S(-II) was not detected. The error bars are standard deviations (SD, $n = 3$).

In the absence of rice roots, no apparent spatial pattern was observed for the As concentration and species across the rhizosphere. The sum of As(III) and As(V) remained at approximately 33.0 $\mu g \cdot L^{-1}$ in the soil porewaters, with an As(III) proportion of 67.6% (Fig. 3). In contrast, in the presence of rice roots, an obvious spatial pattern was detected for As across the rhizosphere. The sum of As(III) and As(V) decreased linearly from 40.5 $\mu g \cdot L^{-1}$ at >10 mm from the root bag surface to as low as 5.93 $\mu g \cdot L^{-1}$ at 0-2 mm around the root bag (Fig. 3). Moreover, the As(III) proportion increased from 65.6% to 89.2% with a decreasing distance from the root bag surface. Fig. 3 clearly illustrates that the rhizosphere retained a relatively high As(III) concentration, while As(V) was almost depleted within 0-4 mm around the root bag. However, the presence or absence of rice roots had an insignificant effect on the S concentration and speciation across the rhizosphere. The S(VI) remained at approximately 180 $mg \cdot L^{-1}$ in the soil porewaters (Fig. 3).

Analysis of the 16S rRNA gene at 0-2 mm from the root bag yielded a high value of Good's coverage (> 0.96, Table S2), indicating that the sequencing was deep enough to cover the bacterial communities. Alpha analysis obtained similar Chao 1 (10253) and Shannon (6.73) values for all treatments. However, principal coordinates analysis of PCoA1 *vs.* PCoA2 (explaining 72.0%) showed that the bacterial communities were different between the two treatments (Fig. 4A). This indicates that growing rice could significantly alter the bacterial community in the rhizosphere. Furthermore, LEfSe analysis identified that some bacterial groups, such as *Bacteroidetes*, *Proteobacteria*, *Acidobacteria*, and *Thiobacillus*, were enriched around the roots (Fig. S3).

To further reveal the potential involvement of biotic regulation of As in the rhizosphere, 19 As genes were investigated by AsChip analysis. In the absence of rice

roots, *aoxB* and *arsC* were the most abundant As genes in the soils (Fig. 4B), while *aoxD* and *arsD* were undetectable. Our results suggested that growing rice significantly increased the abundance of almost all As(III)-oxidizing genes (including *aoxA*/*B*/*C*/*R*/*S*/*H*). This result indicates that biotic As oxidation could be substantially promoted by oxygenation of the rhizosphere via ROL. For As reduction, methylation, and transport, some of their genes were promoted in the rhizosphere, including *arsACIPR*.

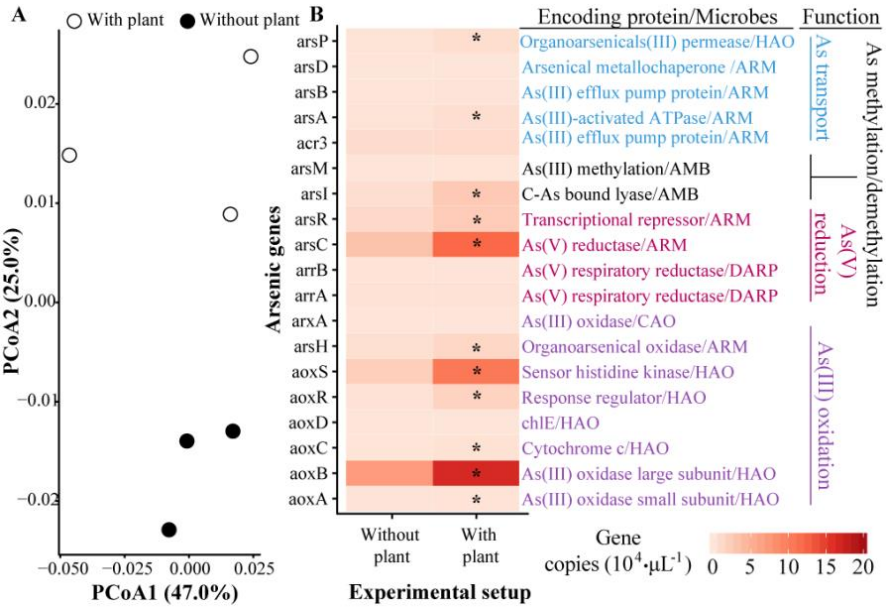

Figure 4 Principal coordinates analysis (PCoA) of the microbial community (A) and the abundances of 19 As genes (B) around root bags at DAF 40. Abbreviations used: HAO, heterotrophic As(III) oxidizers; ARM, As-resistant microorganisms; CAO, chemoautotrophic As(III) oxidizers; DARP, dissimilatory As(V)-reducing prokaryotes. The star represents significance ($p < 0.05$).

Discussions

The element behaviors in the plant rhizosphere have received much attention due to their importance in plant nutrition. However, tracking their dynamic distributions in

406 the rhizosphere is still challenging. A broad view of the spatiotemporal changes in
407 elements in the rice rhizosphere is made possible by using Rhizon profilers.

408 The covariance of elements such as Fe, Mn, As, P, Co and S (Fig. 2) in time and
409 space in the rhizosphere was mainly attributed to the adsorption sites provided by Fe
410 oxides for the noted elements in the rhizosphere (Han et al. 2020; Ilhardt et al. 2019).
411 Fe oxides serve as electron acceptors for dissimilatory Fe-reducing bacteria and are
412 reduced under hypoxic conditions when soils are flooded (Zhang et al. 2012).
413 Meanwhile, the solute-phase elements adsorbed on Fe oxides are re-immobilized by
414 secondary Fe minerals (siderite, troilite, pyrite, and vivianite) after being released
415 under continuous flooding (Borch et al. 2010; Burton et al. 2008; Muehe et al. 2019;
416 Shaheen et al. 2013). Moreover, ROL-induced Fe plaques greatly enhanced the re-
417 immobilization of solute-phase elements in the rice rhizosphere (Maisch et al. 2019).
418 Consequently, the spatiotemporal fluctuation of aqueous Fe, Mn, P, As, S, and Co
419 observed in this study (Fig. 2) could be well explained by the noted interplay between
420 the mobilization and re-immobilization processes. However, such detailed monitoring
421 of multiple elements in the same rhizosphere has not yet been investigated. Previous
422 studies generally reported only one-dimensional spatial or temporal changes in
423 elements (Fulda et al. 2013; Jia et al. 2014; Jia et al. 2013; Muehe et al. 2019;
424 Williams et al. 2014; Yin et al. 2020). In addition, two-dimensional changes in
425 elements, such as with a limited spatial resolution (cm-scale with the Rhizon sampler)
426 and/or measurement range (few parameters with planar optode), have also been
427 previously documented (Bravin et al. 2008; Maisch et al. 2019). However, they failed
428 to reveal the detailed spatiotemporal dynamics of multiple elements in the
429 rhizosphere. The present study achieved this goal by providing an advanced solution

by integrating/utilizing as many associated parameters as possible to deeply investigate element cycling in the rhizosphere.

The collection of fine-scale As species profiles in this study revealed that both As(III) and As(V) were fixed in the rice rhizosphere (Fig. 3). The depletion (~ 1.3 $\mu g \cdot L^{-1}$) of As(V) at 0-4 mm from the root bag surface was attributed to its stronger affinity to Fe oxides than As(III). The depletion of As(V) in this study was attributed to its direct adsorption on Fe plaques (Chen et al. 2005) and the transformation of As(III) to less mobile As(V) followed by its fixation on Fe plaques (Tong et al. 2019). The latter process could be stimulated by both abiotic and biotic As(III) oxidation mediated by ROL and microbes, respectively (Awasthi et al. 2017; Tong et al. 2019). The biotic pathway was supported by the significant promotion of all As oxidizing genes in the rhizosphere (Fig. 4). Despite the presence of methylation genes (*arsM*), no methyl As was detected in the rhizosphere (Fig. 4) or in the plant tissues (Fig. S6). The similar phenomenon was also observed by many studies using As contaminated paddy soils with diverse geographical sources (Xu et al. 2017; Zhao et al. 2013). Previous studies reported that considerable methyl As (mainly DMA) accumulated in rice grains originated from the soil (Lomax et al. 2012; Šlejkovec et al. 2020), since rice plants cannot perform As methylation *in vivo*. A recent study reported that inorganic As was first methylated by S(VI)-reducing bacteria followed by rapid demethylation of methyl As produced by methanogenic archaea under highly reducing conditions during flooding (Chen et al. 2019a). However, the conversion of S(VI) to S(-II) was not observed (Fig. 3), indicating that S(VI)-reducing bacteria were not activated in this study. Consequently, the absence of methyl As might be attributed to the lack of S(VI)-reducing bacteria or other anaerobic microbes processing *arsM* genes.

455 Conversely, aqueous Cd and Sb tended to be immobilized during flooding, and
456 Cd was further remobilized around the root bag (Fig. 2). The rapid decline in Cd and
457 Sb after flooding was attributed to the formation of CdS and Sb_2S_3 (Arsic et al. 2018;
458 Fulda et al. 2013). However, this may not be the case in this study, as significant S(-
459 II) was not detected in the porewater (Fig. 3). We can conclude that the reduction of
460 S(VI) to S(-II) was not activated during the 40-day incubation, and our results are
461 consistent with a previous report indicating that this phenomenon continued until 49
462 days after flooding (Burton et al. 2008). The occurrence of this phenomenon is most
463 likely because S(VI) reduction is much less energy favorable than Fe oxide reduction
464 (Borch et al. 2010). Changes in soil pH were reported to be the major factor
465 governing Cd mobility (Wang et al. 2019). Elevated soil pH induced by Fe oxide
466 reduction could inhibit Cd mobilization under flooding. However, the immobilization
467 of Sb is credited to secondary Fe minerals formed under S(-II)-free reducing
468 conditions (Burton et al. 2019). In contrast, the acidification of the rice rhizosphere,
469 potentially caused by protons generated during Fe^{2+} oxidation and plant exudates
470 (Maisch et al. 2019), could significantly enhance Cd mobilization, which could also
471 be further enhanced by chelating complexes (small organic acids) released by roots
472 (rhizodeposits) (Li et al. 2013). Rhizodeposits could also explain the Zn mobilization
473 observed in this study (Fig. 2). Conversely, As was mostly controlled by the
474 oxidation-mediated development of Fe plaques and was little affected by rhizosphere
475 acidification or rhizodeposits (Bravin et al. 2008).

476 Fe plaques have a high affinity for multiple solutes and are believed to be an
477 important barrier for element uptake and translocation from porewater to plants (Gao
478 et al. 2006; Violante and Pigna 2002; Xu et al. 2017). Therefore, elements in
479 porewater around roots should be used to estimate their supply potential for plants.

However, considerable bias could be introduced if the elemental concentration in bulk soil porewater was utilized to estimate the supply potential. Fe, Mn, P, As, Sb and Co could be overestimated with a bias up to 17.5% - 196%, while Cd and Zn could be underestimated with a bias as high as -54.1% and -27.0%, respectively (Table 1). Considering the significant variation in the elemental translocation coefficient from the bulk soil to the rhizosphere (T_{bs-r}, 0.342-2.38), a well-resolved rhizosphere is essential to predict elemental translocation from rhizosphere to root (T_{r-r}, 6.78-43726), root to stem (T_{r-s}, 0.00975-1.65), stem to leaf (T_{s-l}, 0.241-1.29), and porewater to leaf ($T_{overall}$, 1.93-5875). However, the well-resolved rhizospheric effect was not taken into account in most previous studies on plant nutrition due to a lack of appropriate techniques (Kuzyakov and Razavi 2019; Muehe et al. 2019; Shaheen et al. 2014; Wan et al. 2019). DGT probes and laser-induced breakdown spectroscopy were applied to investigate the well-resolved elements in the rhizosphere (Ilhardt et al. 2019; Williams et al. 2014; Yin et al. 2020); however, they can only provide a snapshot at a certain time point. Snapshot information might be limited in predicting element translocation and accumulation in plants owing to fluctuations in the soil/rhizosphere environment during flooding/root elongation (Chen et al. 2019a; Muehe et al. 2019). Rhizon profilers that are able to provide well-resolved temporal data across the rhizosphere during plant growth could be employed to fully address the aforementioned limitation. The potential limitations of Rhizon profilers may include: i) the sampler could shield the retained soil used for 16S rRNA and qPCR sequencing from rhizospheric effects, due to the soil has a small cross-section (length × width = 2.5 cm × 0.25cm) toward the root bag; ii) the sampler cannot always mark the root edge, especially at the early growth stage when rice roots are not well developed.

Table 1. Translocation of multiple elements from bulk soil porewater to rice leaves

Elements†	Bulk soil porewater	Leaf	Translocation coefficient‡				
			T_{bs-r}	T_{r-r}	T_{r-s}	T_{s-l}	$T_{overall}$
Sb	36.7±2.27	70.8±14.4	0.700±0.059	57.9±19.5	0.077±0.001	0.615±0.122	1.93±0.129
As	112±11.6	358±67.8	0.342±0.016	1354±645	0.010±0.001	0.705±0.133	3.19±0.019
Fe	37.4±3.77	167±33.3	0.369±0.012	1150±636	0.016±0.002	0.679±0.135	4.45±0.179
Co	48.1±1.24	249±63.3	0.852±0.002	125±48.4	0.042±0.006	1.17±0.298	5.18±1.14
S	324±10.2	1692±203	0.914±0.026	6.78±2.49	0.653±0.080	1.29±0.154	5.22±0.534
Mn	7.79±0.303	266±19.3	0.789±0.013	33.7±11.1	1.55±0.117	0.829±0.060	34.2±1.31
Zn	2.45±0.272	111±4.39	1.37±0.213	301±131	0.154±0.032	0.707±0.119	45.2±1.62
Cr	7.57±0.326	646±90.3	1.01±0.013	4816±3278	0.017±0.002	1.02±0.142	85.3±69.0
Cd	0.538±0.104	2297±161	2.38±0.947	43726±13345	0.171±0.017	0.241±0.017	4268±755
P	0.204±0.205	1197±117	0.440±0.051	11296±3640	1.65±0.155	0.716±0.070	5875±310

† The units for Fe, Mn, P and S: $mg \cdot L^{-1}$ (porewater) and $mg \cdot kg^{-1}$ (plant tissues); the units of Sb, As, Co, Zn, Cr and Cd: $\mu g \cdot L^{-1}$ (porewater) and $\mu g \cdot kg^{-1}$ (plant tissues).

‡ Translocation coefficient describes element migration from soil porewater to fresh plant tissues. T_{bs-r}, T_{r-r}, T_{r-s}, T_{s-l} and $T_{overall}$ are translocation coefficients of the element from bulk soil to rhizosphere, rhizosphere to root, root to stem, stem to leaf, and bulk soil to leaf, respectively.

Data are mean±SD (n = 3).

Conclusions

We found that elements in rice plants are taken up from soil porewater in the rhizosphere, which is temporally and spatially determined by multiple biogeochemical processes in soils as well as exudates from plant roots. This is a first attempt to demonstrate two-dimensional (time and space) co-distributions of multiple elements and their species across the paddy rhizosphere with an updated porewater sampler. In addition, the broad view of elemental behaviors from bulk porewater to rhizosphere and then to plant tissues was also illustrated for the first time by combining the collected microbial data with element translocation and accumulation in plants.

However, the reflection of the complex rhizosphere process is still in its infancy. A combination of isotopic labeling, *in situ* high-resolution porewater sampling, non-destructive visualization and deep sequencing techniques could provide a powerful tool to uncover the critical but overlooked rhizosphere processes in future studies.

Acknowledgments

The National Science Foundation of China (41977320, 41571305) and Key Programme Special Fund of XJTLU (KSF-A-20) financially supported this work. We appreciate the outstanding laboratory support from Yi-Li Cheng, Xiao Zhou, Xiao-Yan Zhang, and Liang-Ping Long.

Conflicts of interest

The authors declare no financial conflict.

Data availability

The data from this study will be made available by the authors upon request.

Authors' contributions

Z.C., Z.Y., and W.G. designed research; Z.Y., W.G., and F.L. performed research; Z.C., Z.Y., S.T.A., J.B., R.S., and W.G. wrote the paper.

References

Afroz H, Su S, Carey MP, Meharg AA, Meharg C (2019) Inhibition of microbial methylation via arsM in the rhizosphere: arsenic speciation in the soil to plant continuum. Environ Sci Technol 53: 3451-3463.

Arsic M, Teasdale PR, Welsh DT, Johnston SG, Burton ED, Hockmann K, Bennett WW (2018) Diffusive gradients in thin films (DGT) reveals antimony and arsenic mobility differs in a contaminated wetland sediment during an oxic-anoxic transition. Environ Sci Technol 52: 1118-1127.

Awasthi S, Chauhan R, Srivastava S, Tripathi RD (2017) The journey of arsenic from soil to grain in rice. Front Plant Sci 8: 1007.

Borch T, Kretzschmar R, Kappler A, Cappellen PV, Gindervogel M, Voegelin A, Campbell K (2010) Biogeochemical redox processes and their impact on contaminant dynamics. Environ Sci Technol 44: 15-23.

556 Brackin R, Atkinson BS, Sturrock CJ, Rasmussen A (2017) Roots-eye view: Using
557 microdialysis and microCT to non-destructively map root nutrient depletion and
558 accumulation zones. Plant Cell Environ 40: 3135-3142.
559 Bravin MN, Travassac F, Le Floch M, Hinsinger P, Garnier J-M (2008) Oxygen input
560 controls the spatial and temporal dynamics of arsenic at the surface of a flooded
561 paddy soil and in the rhizosphere of lowland rice (*Oryza sativa* L.): a microcosm
562 study. Plant soil 312: 207-218.
563 Burton ED, Bush RT, Sullivan LA, Johnston SG, Hocking RK (2008) Mobility of arsenic
564 and selected metals during re-flooding of iron- and organic-rich acid-sulfate soil.
565 Chem Geol 253: 64-73.
566 Burton ED, Hockmann K, Karimian N, Johnston SG (2019) Antimony mobility in
567 reducing environments: The effect of microbial iron (III)-reduction and associated
568 secondary mineralization. Geochim Cosmochim Ac 245: 278-289.
569 Chen C, Li L, Huang K, Zhang J, Xie WY, Lu Y, Dong X, Zhao FJ (2019a) Sulfate-
570 reducing bacteria and methanogens are involved in arsenic methylation and
571 demethylation in paddy soils. ISME J 13: 2523-2535.
572 Chen H, Lei J, Tong H, Gu M, Fang Y, Wang X, Tang C, Li Z, Liu C (2019b) Effects of
573 Mn(II) on theoxidation of Fe in soils and the uptake of cadmium by rice (*Oryza*
574 *sativa*). Water, Air, Soil Pollut 230: 190.
575 Chen Q, An X, Li H, Su J, Ma Y, Zhu Y (2016) Long-term field application of sewage
576 sludge increases the abundance of antibiotic resistance genes in soil. Environ Int
577 92: 1-10.

578 Chen Z, Huang YC, Liang JH, Zhao F, Zhu YG (2012) A novel sediment microbial fuel
579 cell with a biocathode in the rice rhizosphere. Bioresource Technol 108: 55-59.
580 Chen Z, Zhu YG, Liu WJ, Meharg AA (2005) Direct evidence showing the effect of root
581 surface iron plaque on arsenite and arsenate uptake into rice (*Oryza sativa*) roots.
582 New Phytol 165: 91-97.
583 Eberle A, Besold J, Kerl CF, Lezama-Pacheco JS, Fendorf S, Planer-Friedrich B (2020)
584 Arsenic fate in peat controlled by the pH-dependent role of reduced sulfur.
585 Environ Sci Technol 54: 6682-6692.
586 Fulda B, Voegelin A, Kretzschmar R (2013) Redox-controlled changes in cadmium
587 solubility and solid-phase speciation in a paddy soil as affected by reducible
588 sulfate and copper. Environ Sci Technol 47: 12775-12783.
589 Gao Y, Leermakers M, Gabelle C, Divis P, Billon G, Ouddane B, Fischer JC, Wartel M,
590 Baeyens W (2006) High-resolution profiles of trace metals in the pore waters of
591 riverine sediment assessed by DET and DGT. Sci Total Environ 362: 266-277.
592 Guo T, Gustave W, Lu H, He Y, Tang X, Buchwalter DB, Xu J (2020) Periphyton
593 enhances arsenic release and methylation at the soil-water interface of paddy
594 soils. J Hazard Mater: 124946.
595 Gustave W, Yuan ZF, Ren YX, Sekar R, Chen Z (2019) Arsenic alleviation in rice by
596 using paddy soil microbial fuel cells. Plant Soil 441: 111-127.
597 Han J, Kim M, Ro H-M (2020) Factors modifying the structural configuration
598 of oxyanions and organic acids adsorbed on iron (hydr)oxides in soils. A review.
599 Environ Chem Lett 18: 631-662.

600 Hansel CM, Fendorf S, Sutton S, Newville M (2001) Characterization of Fe plaque and
601 associated metals on the roots of mine-waste impacted aquatic plants. Environ Sci
602 Technol 35: 3863-3868.
603 Ilhardt PD, Nuñez JR, Denis EH, Rosnow JJ, Krogstad EJ, Renslow RS, Moran JJ (2019)
604 High-resolution elemental mapping of the root-rhizosphere-soil continuum using
605 laser-induced breakdown spectroscopy (LIBS). Soil Biol Biochem 131: 119-132.
606 Jia Y, Huang H, Chen Z, Zhu YG (2014) Arsenic uptake by rice is influenced by
607 microbe-mediated arsenic redox changes in the rhizosphere. Environ Sci Technol
608 48: 1001-1007.
609 Jia Y, Huang H, Zhong M, Wang FH, Zhang LM, Zhu YG (2013) Microbial arsenic
610 methylation in soil and rice rhizosphere. Environ Sci Technol 47: 3141-3148.
611 Kumarathilaka P, Seneweera S, Meharg A, Bundschuh J (2018) Arsenic speciation
612 dynamics in paddy rice soil-water environment: sources, physico-chemical, and
613 biological factors-a review. Water Res 140: 403-414.
614 Kuzyakov Y, Razavi BS (2019) Rhizosphere size and shape: Temporal dynamics and
615 spatial stationarity. Soil Biol Biochem 135: 343-360.
616 Li T, Tao Q, Liang C, Shohag MJI, Yang X, Sparks DL (2013) Complexation with
617 dissolved organic matter and mobility control of heavy metals in the rhizosphere
618 of hyperaccumulator Sedum alfredii. Environ Pollut 182: 248-255.
619 Liu HJ, Zhang JL, Zhang FS (2007) Role of iron plaque in Cd uptake by and
620 translocation within rice (*Oryza sativa* L.) seedlings grown in solution culture.
621 Environ Exp Bot 59: 314-320.

622 Lomax C, Liu W, Wu L, Xue K, Xiong J, Zhou J, McGrath SP, Meharg AA, Miller AJ,
623 Zhao F (2012) Methylated arsenic species in plants originate from soil
624 microorganisms. New Phytol 193: 665-672.
625 Ma X, Liu J, Wang M (2012) Differences between rice cultivars in iron plaque formation
626 on roots and plant lead tolerance. Adv J Food Sci Technol 5: 160-163.
627 Maisch M, Lueder U, Kappler A, Schmidt C (2019) Iron lung: how rice roots induce iron
628 redox changes in the rhizosphere and create niches for microaerophilic Fe (II)-
629 oxidizing bacteria. Environ Sci Technol Lett 6: 600-605.
630 Martin BC, Bougoure J, Ryan MH, Bennett WW, Colmer TD, Joyce NK, Olsen YS,
631 Kendrick GA (2019) Oxygen loss from seagrass roots coincides with colonisation
632 of sulphide-oxidising cable bacteria and reduces sulphide stress. ISME J 13: 707.
633 Muehe EM, Wang T, Kerl CF, Planer-Friedrich B, Fendorf S (2019) Rice production
634 threatened by coupled stresses of climate and soil arsenic. Nat Commun 10: 1-10.
635 Pester M, Knorr KH, Friedrich MW, Wagner M, Loy A (2012) Sulfate-reducing
636 microorganisms in wetlands-fameless actors in carbon cycling and climate
637 change. Front Microbiol 3: 72.
638 Quaghebeur M, Rengel Z, Smirk M (2003) Arsenic speciation in terrestrial plant material
639 using microwave-assisted extraction, ion chromatography and inductively coupled
640 plasma mass spectrometry. J Anal Atom Spectrom 18: 128-134.
641 Revsbech NP, Pedersen O, Reichardt W, Briones A (1999) Microsensor analysis of
642 oxygen and pH in the rice rhizosphere under field and laboratory conditions. Biol
643 Fertil Soils 29: 379-385.

644 Richardson AE, Barea JM, McNeill AM, Prigent Combaret C (2009) Acquisition of
645 phosphorus and nitrogen in the rhizosphere and plant growth promotion by
646 microorganisms. Plant Soil 321: 305-339.
647 Seeberg-Elverfeldt J, Schlüter M, Feseker T, Kölling M (2005) Rhizon sampling of
648 porewaters near the sediment-water interface of aquatic systems. Limnol
649 Oceanogr-Meth 3: 361-371.
650 Segata N, Izard J, Waldron L, Gevers D, Miropolsky L, Garrett WS, Huttenhower C
651 (2011) Metagenomic biomarker discovery and explanation. Genome Biol 12:
652 R60.
653 Shaheen SM, Rinklebe J, Rupp H, Meissner R (2014) Temporal dynamics of pore water
654 concentrations of Cd, Co, Cu, Ni, and Zn and their controlling factors in a
655 contaminated floodplain soil assessed by undisturbed groundwater lysimeters.
656 Environ Pollut 191: 223-231.
657 Shaheen SM, Tsadilas CD, Rinklebe J (2013) A review of the distribution coefficients of
658 trace elements in soils: Influence of sorption system, element characteristics, and
659 soil colloidal properties. Adv Colloid Interface 201: 43-56.
660 Šlejkovec Z, Gorše L, Grobler A, Jagodic M, Falnoga I (2020) Arsenic speciation and
661 elemental composition of rice samples from the Slovenian market. Food Chem:
662 128348.
663 Suda A, Makino T (2016) Functional effects of manganese and iron oxides on the
664 dynamics of trace elements in soils with a special focus on arsenic and cadmium:
665 A review. Geoderma 270: 68-75.

666 Suzuki Y, Shimoda Y, Endo Y, Hata A, Yamanaka K, Endo G (2009) Rapid and
667 effective speciation analysis of arsenic compounds in human urine using anion-
668 exchange columns in HPLC-ICP-MS. J Occup Health 51: 380-385.
669 Thomas F, Giblin AE, Cardon ZG, Sievert SM (2014) Rhizosphere heterogeneity shapes
670 abundance and activity of sulfur-oxidizing bacteria in vegetated salt marsh
671 sediments. Front Microbiol 5.
672 Tong H, Liu C, Hao L, Swanner ED, Chen M, Li F, Xia Y, Liu Y, Liu Y (2019)
673 Biological Fe(II) and As(III) oxidation immobilizes arsenic in micro-oxic
674 environments. Geochim Cosmochim Ac 265: 96-108.
675 Violante A, Pigna M (2002) Competitive sorption of arsenate and phosphate on different
676 clay minerals and soils. Soil Sci Soc Am J 66: 1788-1796.
677 Wan Y, Huang Q, Camara AY, Wang Q, Li H (2019) Water management impacts on the
678 solubility of Cd, Pb, As, and Cr and their uptake by rice in two contaminated
679 paddy soils. Chemosphere 228: 360-369.
680 Wang J, Wang PM, Gu Y, Kopittke PM, Zhao FJ, Wang P (2019) Iron–manganese
681 (oxyhydro)oxides, rather than oxidation of sulfides, determine mobilization of Cd
682 during soil drainage in paddy soil systems. Environ Sci Technol 53: 2500-2508.
683 Williams PN, Santner J, Larsen M, Lehto NJ, Oburger E, Wenzel W, Glud RN, Davison
684 W, Zhang H (2014) Localized flux maxima of arsenic, lead, and iron around root
685 apices in flooded lowland rice. Environ Sci Technol 48: 8498-8506.
686 Xu B, Yu S, Ding J, Wu S, Ma J (2015) Metal-dependent root iron plaque effects on
687 distribution and translocation of chromium and nickel in yellow flag (*Iris*
688 *pseudacorus* L.). Int J Phytoremediat 17: 175-181.

689 Xu X, Chen C, Wang P, Kretzschmar R, Zhao FJ (2017) Control of arsenic mobilization
690 in paddy soils by manganese and iron oxides. Environ Pollut 231: 37-47.
691 Ye ZH, Cheung KC, Wong MH (2001) Copper uptake in *Typha latifolia* as affected by
692 iron and manganese plaque on the root surface. Can J Botany 79: 314-320.
693 Yin DX, Fang W, Guan DX, Williams PN, Moreno Jimenez E, Gao Y, Zhao FJ, Ma LQ,
694 Zhang H, Luo J (2020) Localized intensification of arsenic release within the
695 emergent rice rhizosphere. Environ Sci Technol 54: 3138-3147.
696 Yuan ZF, Gustave W, Boyle J, Sekar R, Bridge J, Ren Y, Tang X, Guo B, Chen Z (2020)
697 Arsenic behavior across soil-water interfaces in paddy soils: coupling, decoupling
698 and speciation. Chemosphere: 128713.
699 Yuan ZF, Gustave W, Bridge J, Liang Y, Sekar R, Boyle J, Jin CY, Pu TY, Ren YX,
700 Chen Z (2019) Tracing the dynamic changes of element profiles by novel soil
701 porewater samplers with ultralow disturbance to soil-water interface. Environ Sci
702 Technol 53: 5124-5132.
703 Yuan ZF, Gustave W, Sekar R, Bridge J, Wang JY, Feng WJ, Guo B, Chen Z (2021)
704 Simultaneous measurement of aqueous redox-sensitive elements and their species
705 across the soil-water interface. J Environ Sci 102: 1-10.
706 Zhang C, Ge Y, Yao H, Chen X, Hu M (2012) Iron oxidation-reduction and its impacts
707 on cadmium bioavailability in paddy soils: a review. Front Envi Sci Eng 6: 509-
708 517.
709 Zhang X, Zhang F, Mao D (1999) Effect of iron plaque outside roots on nutrient uptake
710 by rice (*Oryza sativa* L.): Phosphorus uptake. Plant Soil 209: 187-192.

711 Zhao FJ, Harris E, Yan J, Ma J, Wu L, Liu W, McGrath SP, Zhou J, Zhu YG (2013)
712 Arsenic methylation in soils and its relationship with microbial arsM abundance
713 and diversity, and As speciation in rice. Environ Sci Technol 47: 7147-7154.
714 Zhao Y, Su J, Ye J, Rensing C, Tardif S, Zhu Y, Brandt KK (2019) AsChip: a high-
715 throughput qPCR chip for comprehensive profiling of genes linked to microbial
716 cycling of arsenic. Environ Sci Technol 53: 798-807.